Atmospheric Mercury in Vermont and New England:
Measurement of deposition, surface exchanges and assimilation in terrestrial ecosystems

Final Project Report – Ambient Air Mercury Speciation Studies – 1/16/2009

PI: Melody Brown Burkins, University of Vermont (UVM)
Co-PIs: Eric K. Miller[1], Ecosystems Research Group, Ltd.; and Jamie Shanley, US Geological Survey
Collaborators: Sean Lawson, VTANR-VMC; Mim Pendelton, Carl Waite, UVM;
      Rich Poirot, VTANR-APCD; Alan VanArsdale, USEPA; Mark Cohen, NOAA
Project Officer: Eric Hall, USEPA

Climatology and potential sources of speciated (GEM, RGM, and HGP) ambient atmospheric mercury in Northern New England

Earlier modeling studies indicated that RGM deposition could be nearly equal in magnitude to the wet deposition flux of Hg (Miller et al. 2005). At the outset of this project, there were few measurements of RGM levels in the US (e.g. Lindberg and Stratton 1998) and none in rural northern New England. The Vermont Agency of Natural Resources Air Pollution Control Division (VTANR-APCD) funded the acquisition of a Tekran 1130 RGM module for use with the Tekran 2537A as part of this project. The Tekran 1130 RGM module was deployed with the Tekran 2537A with inlets on the top of the forest canopy observation tower in 2004. This tower was destroyed in a severe storm in the winter of 2004 and equipment was repaired and relocated to the Underhill Air Quality site in the spring of 2005. We acquired and deployed an 1135 particulate mercury module in 2005. We also conducted one short-term deployment of a second system provide by USEPA Region 1 at Shoreham, VT, allowing paired observations at a lake-level and mid-elevation site (see FR-sec3b). These measurements were designed to characterize GEM, RGM, and HGP levels in terms of their diurnal, seasonal and spatial variation in the region. The measurements provided necessary information for dry-deposition modeling as well as the opportunity for analysis of potential mercury sources using air-mass back-trajectory methods.

Ambient TGM had been characterized at Underhill since 1992 using 24-hour exposures of gold traps every 6th day (Burke et al. 1995). The Tekran system provided continuous hourly (or more frequent) measurements of TGM (or GEM) providing valuable information on TGM/GEM levels allowing us to characterize the diurnal and seasonal variation in this parameter.

GEM and RGM measurements were initiated in 2004 with inlets located at the top of the forest canopy observation tower (Figure 1). Due to the collapse of the forest canopy tower in a severe storm during December 2004, RGM and GEM measurements were relocated to the Air Quality Site (Figure 2). The Air Quality Site is ~1 km from the forest canopy tower site. The basic met package that was previously deployed at the forest canopy tower was redeployed with the vapor-phase mercury instrumentation at the Air Quality Site. A Tekran 1135 particulate mercury sampling head (seen above the 1130 RGM head in Figure 2) for the mercury speciation system was acquired and installed in order to test hypotheses about the influence of $PM_{2.5}$ and humidity on RGM levels. Gathering of this information was necessary to support the deposition-modeling task. The high temporal resolution measurements of mercury speciation also made possible potential

---

[1] Corresponding author for the final project report. Email: ekmiller at ecosystems-research.com Voice: 802-649-5550

source contribution analysis and identification of likely major anthropogenic emissions sources contributing to mercury deposition in the Lake Champlain Basin and Northern New England.

Because of concerns about the comparability of measurements made from the differing inlet locations and heights from 2004 to 2005, the climatology of speciated mercury is presented based on measurements made from the longer, continuous record at the Air Quality Site. Measurements are reported from the period May 2005 through June 2008. GEM measurements were made every 5 minutes during the RGM and HGP 2-hour accumulation periods. GEM concentrations presented below are 2-hour averages of the 5-minute observations to be consistent with the 2-hour average concentrations represented by the RGM and HGP measurements.

RGM Sampling Head

Denuder Inlet   Heated Line

Figure 1. Initial deployment of RGM sampling head on the forest canopy observation tower in 2004.

Figure 2. Sampling heads for RGM, GEM, and particulate mercury were located on the met tower fixed to the instrument shelter (see inset) at the Underhill, VT Air Quality Site in April of 2005.

Climatology of Speciated Ambient Atmospheric Mercury at Underhill, VT

Because we are still uncertain of the comparability of measurements (primarily an issue for RGM) made from the top of the forest canopy tower and from the Air Quality Site, the climatology of speciated mercury is presented based on measurements from the Air Quality Site only. Measurements are reported from the period May 2005 through June 2008. GEM measurements were made every 5 minutes during the RGM and HGP 2-hour accumulation periods. GEM concentrations presented below are 2-hour averages of the 5-minute observations to be consistent with the 2-hour average concentrations represented by the RGM and HGP measurements.

GEM concentrations ranged from 0.81 to 5.58 ng/m3 with a period average of 1.45 ng/m^3 (Figure 3). RGM concentrations ranged from 0 to 132.5 pg/m^3 with a period average of 3.56 pg/m^3 (Figure 3). HGP sampling spanned only 44% of the RGM measurement period due to the later acquisition date of the 1135 module, deployment at Shoreham, VT, and minor problems with the module (Table 1). HGP concentrations ranged from 0 to 121 pg/m^3 with a period average of 11.50 pg/m^3 (Figure 3).

Table 1. Numbers of RGM and HGP 2-hour samples.

Month	N RGM Samples	N HGP Samples	%RGM Samples
1	679	208	30.6
2	622	191	30.7
3	705	194	27.5
4	616	431	70
5	925	479	51.8
6	906	456	50.3
7	663	366	55.2
8	682	440	64.5
9	621	226	36.4
10	713	242	33.9
11	641	240	37.4
12	523	114	21.8

The observed concentrations of all three species were dependent on meteorological conditions but in different ways for RGM and HGP than for GEM. Observed concentrations of all three species were dependent the surface moisture status (dry, moist, or wet) as determined by a Campbell Scientific, Inc. (Logan, Utah) surface wetness sensing grid (2-m AGL, facing SW, 45°-tilt). Mean RGM and HGP concentrations were significantly different for each surface wetness state (dry > moist > wet) (Figure 4). These differences likely exist, in part, because RGM and HGP are more efficiently removed from the atmosphere during wet or moist conditions. Deposition velocities for both species are greater to moist surfaces. Both species tend to exhibit higher concentrations in drier air masses (Figure 5). RGM was more highly correlated with relative humidity than with water-vapor mixing ratio, whereas HGP was more strongly correlated with water vapor mixing ratio. The dependence of RGM concentrations on RH may reflect the tendency for that species to be readily scavenged by moist aerosols at moderate RH. The dependence of HGP on the water vapor mixing ratio may relate to the coincidence of HGP source regions, low water-vapor source regions and seasonal effects (discussed below).

Mean GEM concentrations were significantly higher during moist conditions than either dry or wet for which GEM concentrations were not significantly different. This different response to surface moisture may exist because GEM appears to be volatilized and emitted from moist surfaces in the presence of sunlight (see further discussion below). Short-term increases in GEM were frequently observed at first insolation of moist surfaces (in morning or after precipitation).

8/28/08 11:32 AM
Data Table=VT99-HG-met-EDAS-tstats72h-2005-2008
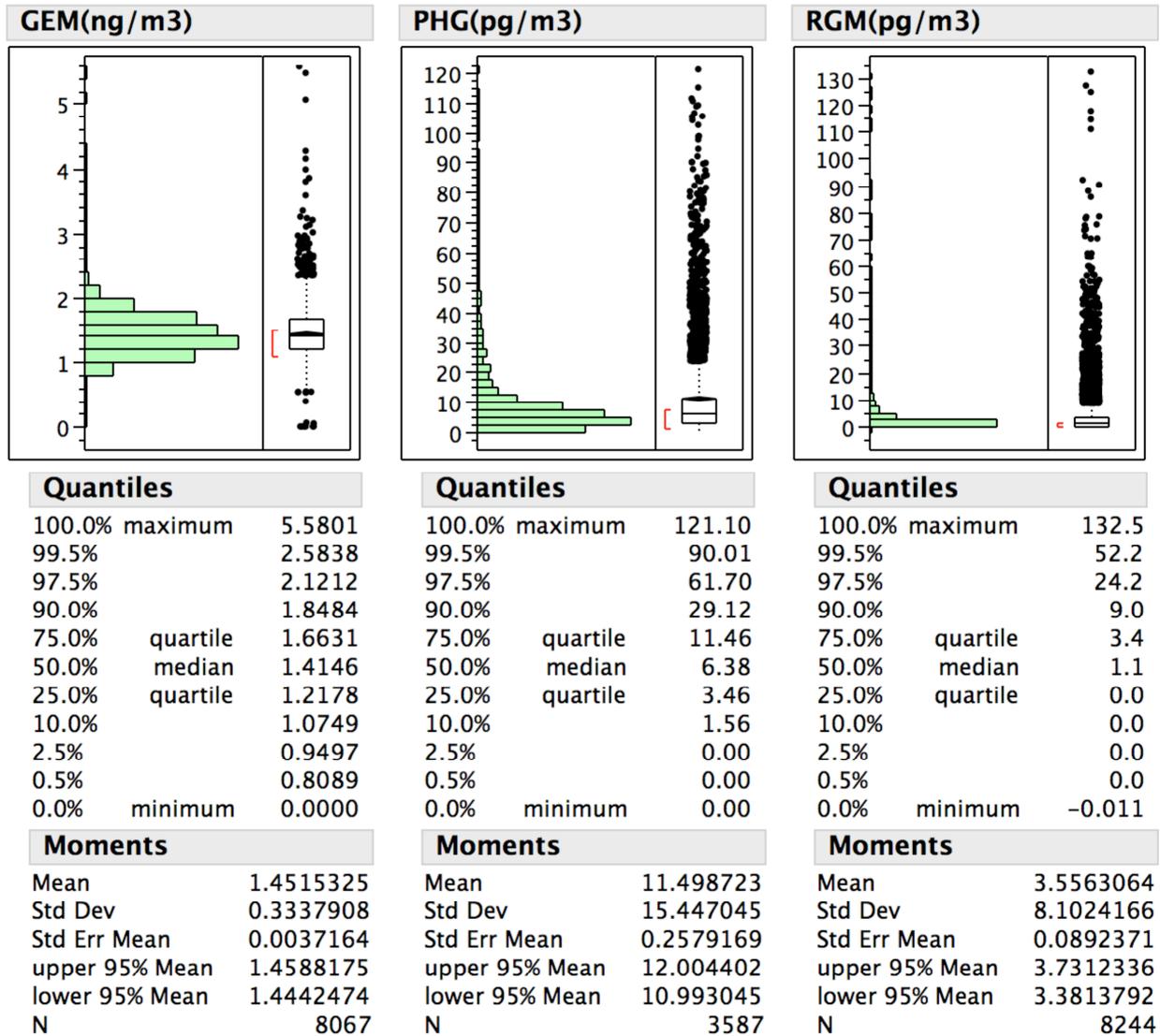
Distributions

GEM(ng/m3)	PHG(pg/m3)	RGM(pg/m3)

GEM(ng/m3)

Quantiles

100.0%	maximum	5.5801
99.5%		2.5838
97.5%		2.1212
90.0%		1.8484
75.0%	quartile	1.6631
50.0%	median	1.4146
25.0%	quartile	1.2178
10.0%		1.0749
2.5%		0.9497
0.5%		0.8089
0.0%	minimum	0.0000

Moments

Mean	1.4515325
Std Dev	0.3337908
Std Err Mean	0.0037164
upper 95% Mean	1.4588175
lower 95% Mean	1.4442474
N	8067

PHG(pg/m3)

Quantiles

100.0%	maximum	121.10
99.5%		90.01
97.5%		61.70
90.0%		29.12
75.0%	quartile	11.46
50.0%	median	6.38
25.0%	quartile	3.46
10.0%		1.56
2.5%		0.00
0.5%		0.00
0.0%	minimum	0.00

Moments

Mean	11.498723
Std Dev	15.447045
Std Err Mean	0.2579169
upper 95% Mean	12.004402
lower 95% Mean	10.993045
N	3587

RGM(pg/m3)

Quantiles

100.0%	maximum	132.5
99.5%		52.2
97.5%		24.2
90.0%		9.0
75.0%	quartile	3.4
50.0%	median	1.1
25.0%	quartile	0.0
10.0%		0.0
2.5%		0.0
0.5%		0.0
0.0%	minimum	−0.011

Moments

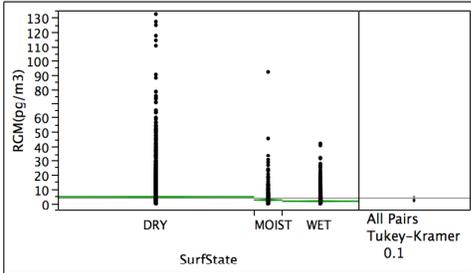| Mean	3.5563064
Std Dev	8.1024166
Std Err Mean	0.0892371
upper 95% Mean	3.7312336
lower 95% Mean	3.3813792
N	8244

Figure 3. Frequency distributions of ambient atmospheric mercury species measured at Underhill, VT from May 2005 through June 2008.

8/28/08 1:39 PM
Data Table=VT99-HG-met-EDAS-tstats72h-2005-2008

Oneway Analysis of RGM(pg/m3) By SurfState

Missing Rows   756

Oneway Anova

Summary of Fit

Rsquare	0.029953
Adj Rsquare	0.029695
Root Mean Square Error	7.951066
Mean of Response	3.568873
Observations (or Sum Wgts)	7540

Analysis of Variance

Source	DF	Sum of Squares	Mean Square	F Ratio	Prob > F
SurfState	2	14712.80	7356.40	116.3629	<.0001*
Error	7537	476485.00	63.22		
C. Total	7539	491197.80			

Means for Oneway Anova

Level	Number	Mean	Std Error	Lower 90%	Upper 90%
DRY	4921	4.57467	0.11334	4.3882	4.7611
MOIST	710	2.30429	0.29840	1.8134	2.7952
WET	1909	1.44648	0.18198	1.1471	1.7458

Std Error uses a pooled estimate of error variance

Means Comparisons

Comparisons for all pairs using Tukey-Kramer HSD

Level		Mean
DRY	A	4.5746653
MOIST	B	2.3042930
WET	C	1.4464767

Levels not connected by same letter are significantly different.

8/28/08 1:40 PM
Data Table=VT99-HG-met-EDAS-tstats72h-2005-2008

Oneway Analysis of PHG(pg/m3) By SurfState
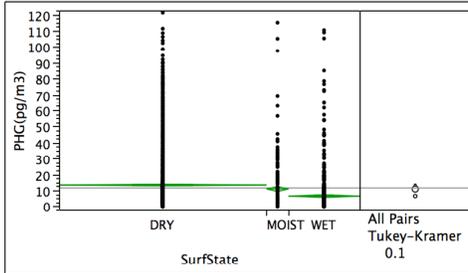
Missing Rows   4718

Oneway Anova

Summary of Fit

Rsquare	0.035181
Adj Rsquare	0.034642
Root Mean Square Error	15.19357
Mean of Response	11.49329
Observations (or Sum Wgts)	3578

Analysis of Variance

Source	DF	Sum of Squares	Mean Square	F Ratio	Prob > F
SurfState	2	30092.86	15046.4	65.1799	<.0001*
Error	3575	825269.65	230.8		
C. Total	3577	855362.51			

Means for Oneway Anova

Level	Number	Mean	Std Error	Lower 90%	Upper 90%
DRY	2470	13.3057	0.30571	12.803	13.809
MOIST	262	10.8214	0.93866	9.277	12.366
WET	846	6.4099	0.52237	5.550	7.269

Std Error uses a pooled estimate of error variance

Means Comparisons

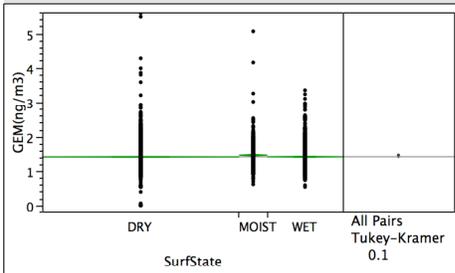**Comparisons for all pairs using Tukey-Kramer HSD**

Level		Mean
DRY	A	13.305672
MOIST	B	10.821363
WET	C	6.409908

Levels not connected by same letter are significantly different.

8/28/08 1:43 PM
Data Table=VT99-HG-met-EDAS-tstats72h-2005-2008

Oneway Analysis of GEM(ng/m3) By SurfState

Missing Rows   927

Oneway Anova

Summary of Fit

Rsquare	0.001996
Adj Rsquare	0.001725
Root Mean Square Error	0.327064
Mean of Response	1.431218
Observations (or Sum Wgts)	7369

Analysis of Variance

Source	DF	Sum of Squares	Mean Square	F Ratio	Prob > F
SurfState	2	1.57567	0.787836	7.3649	0.0006*
Error	7366	787.94846	0.106971		
C. Total	7368	789.52414			

Means for Oneway Anova

Level	Number	Mean	Std Error	Lower 90%	Upper 90%
DRY	4829	1.42579	0.00471	1.4180	1.4335
MOIST	686	1.47671	0.01249	1.4562	1.4973
WET	1854	1.42853	0.00760	1.4160	1.4410

Std Error uses a pooled estimate of error variance

Means Comparisons

Comparisons for all pairs using Tukey-Kramer HSD

Level		Mean
MOIST	A	1.4767123
WET	B	1.4285276
DRY	B	1.4257874

Levels not connected by same letter are significantly different.

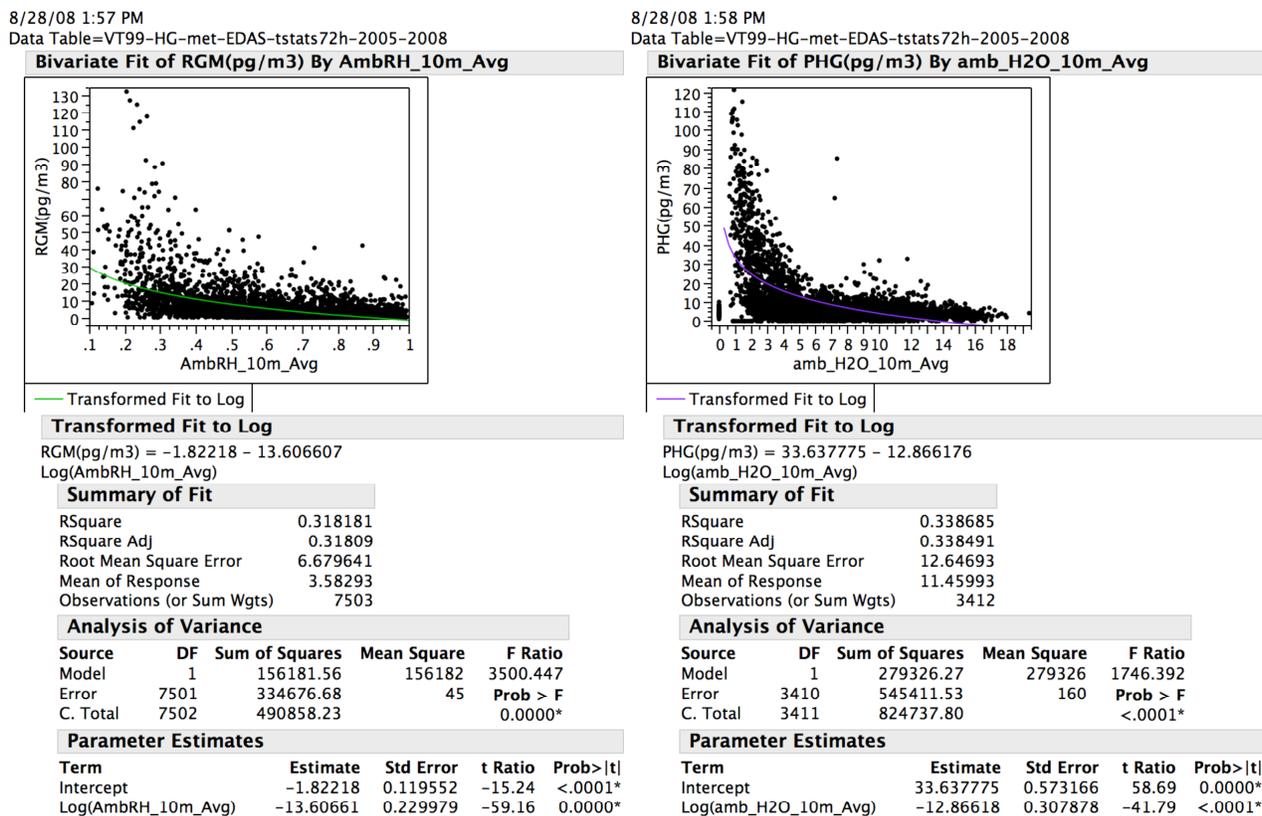**Figure 4.** Ambient atmospheric mercury concentrations by surface wetness class.

8/28/08 1:57 PM
Data Table=VT99-HG-met-EDAS-tstats72h-2005-2008

Bivariate Fit of RGM(pg/m3) By AmbRH_10m_Avg

— Transformed Fit to Log

Transformed Fit to Log

RGM(pg/m3) = −1.82218 − 13.606607
Log(AmbRH_10m_Avg)

Summary of Fit

RSquare	0.318181
RSquare Adj	0.31809
Root Mean Square Error	6.679641
Mean of Response	3.58293
Observations (or Sum Wgts)	7503

Analysis of Variance

Source	DF	Sum of Squares	Mean Square	F Ratio
Model	1	156181.56	156182	3500.447
Error	7501	334676.68	45	Prob > F
C. Total	7502	490858.23		0.0000*

Parameter Estimates

Term	Estimate	Std Error	t Ratio	Prob>|t|
Intercept	−1.82218	0.119552	−15.24	<.0001*
Log(AmbRH_10m_Avg)	−13.60661	0.229979	−59.16	0.0000*

8/28/08 1:58 PM
Data Table=VT99-HG-met-EDAS-tstats72h-2005-2008

Bivariate Fit of PHG(pg/m3) By amb_H2O_10m_Avg

— Transformed Fit to Log

Transformed Fit to Log

PHG(pg/m3) = 33.637775 − 12.866176
Log(amb_H2O_10m_Avg)

Summary of Fit

RSquare	0.338685
RSquare Adj	0.338491
Root Mean Square Error	12.64693
Mean of Response	11.45993
Observations (or Sum Wgts)	3412

Analysis of Variance

Source	DF	Sum of Squares	Mean Square	F Ratio
Model	1	279326.27	279326	1746.392
Error	3410	545411.53	160	Prob > F
C. Total	3411	824737.80		<.0001*

Parameter Estimates

Term	Estimate	Std Error	t Ratio	Prob>|t|
Intercept	33.637775	0.573166	58.69	0.0000*
Log(amb_H2O_10m_Avg)	−12.86618	0.307878	−41.79	<.0001*

Figure 5. Dependence of RGM (left) and HGP (right) on atmospheric moisture. RGM was more highly correlated with relative humidity than with water vapor mixing ratio whereas HGP was more strongly correlated with water vapor mixing ratio (units in figure are mm/mole).

The concentrations of the three mercury species exhibited strong seasonal patterns that were slightly out of phase with each other (Figure 6). GEM concentrations peak in winter and spring with an early fall minimum, HGP concentrations peak in late winter and RGM concentrations peak in spring (Figure 7). The wintertime peak in HGP may be due, in part, to increased local combustion (wood and oil) for home heating. However, trajectory analysis (discussed below) also indicates major out-of-region sources likely contribute to the observed HGP signal. The spring peak in RGM is likely due to a combination of factors including favored trajectories over major EGU RGM sources and relatively low atmospheric moisture levels at a time when leaves are off of trees along the favored trajectories (Figure 8). As soon as leaves emerge in late spring and early summer, the surface area for dry-deposition removal along the transport pathway increases by a factor of 3 to 4. Atmospheric moisture and relative humidity increase as well, allowing more scavenging by particles and ultimately cloud and rain droplets (Figure 9). As discussed in the section on wet-deposition, summer is the time of peak observed concentrations of Hg in precipitation. The patterns described here suggest more of the ionic mercury in the atmosphere is partitioned into the liquid phase during the summer months.
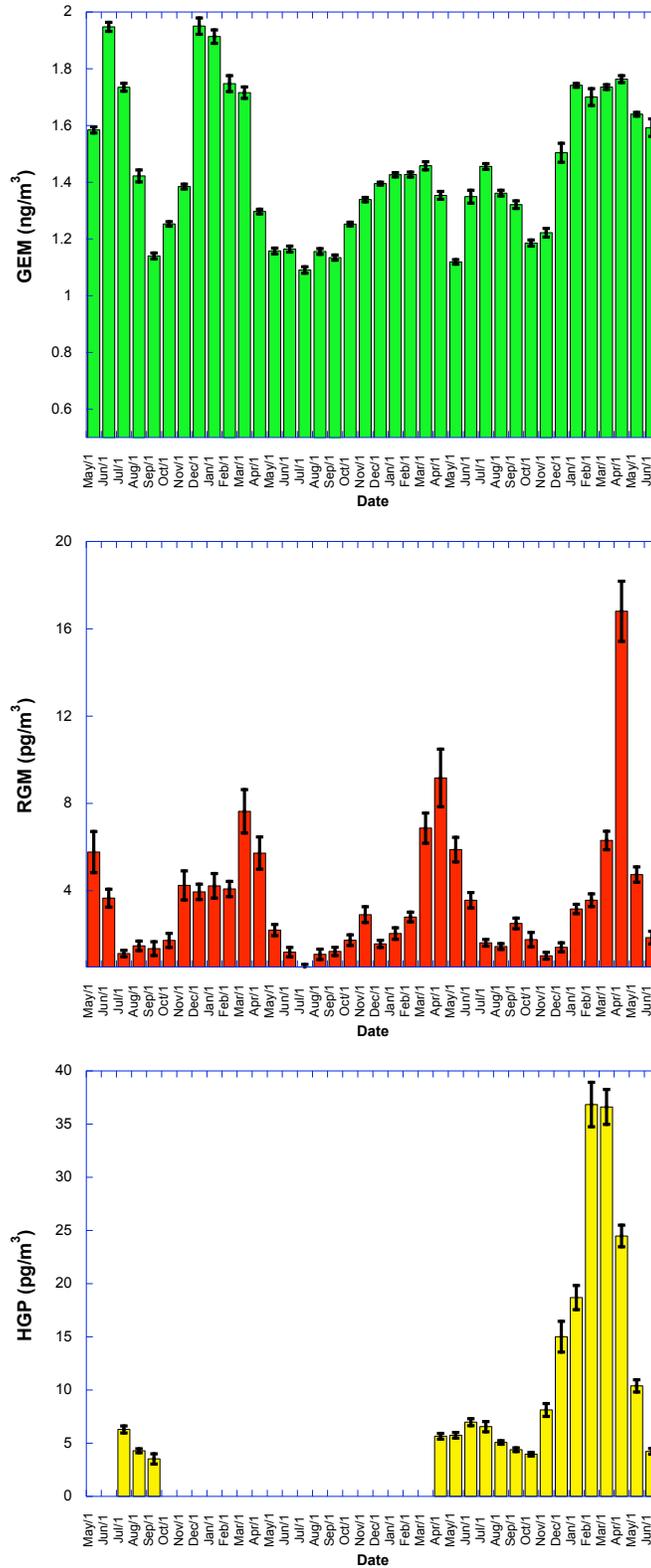
Figure 6. Time series of monthly average concentrations with standard errors for GEM (top), RGM (middle), and HGP (bottom) starting in May of 2005 and ending June 2008. GEM concentrations peak in winter and spring, HGP concentrations peak in late winter and RGM concentrations peak in spring.
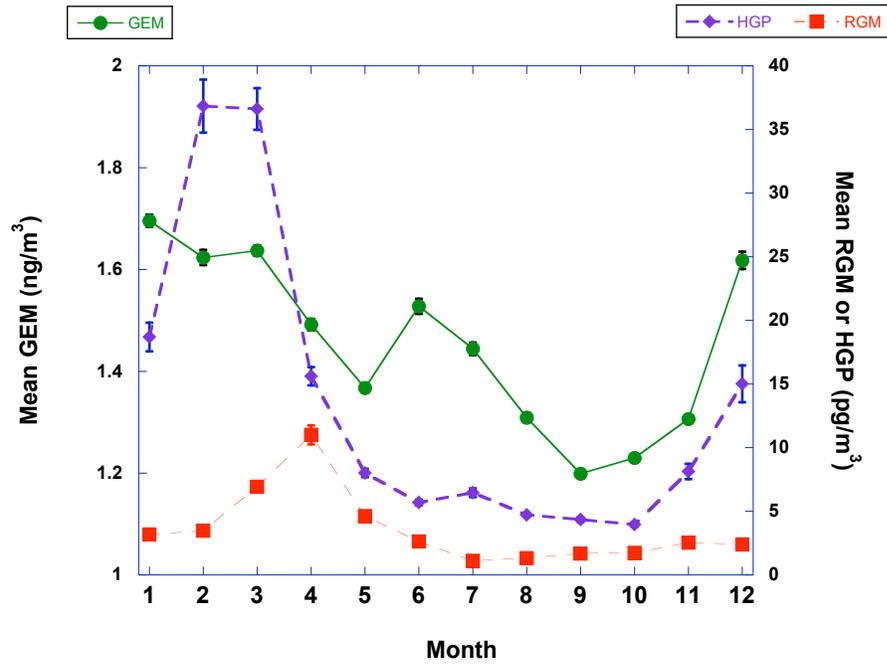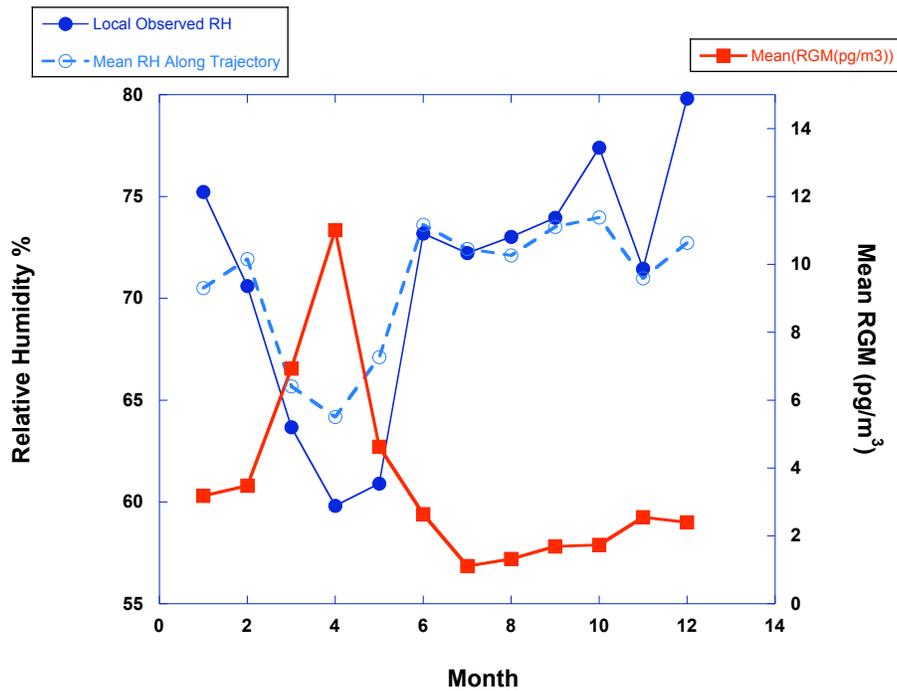
Figure 7. Mean monthly concentrations of atmospheric mercury species over the observation period. GEM concentrations peak in winter and spring with an early fall minimum, HGP concentrations peak in late winter and RGM concentrations peak in spring.

Figure 8. Mean monthly RGM concentrations and mean monthly RH. Both local-observed RH (solid blue line) and the mean of RH values along all back-trajectories for the month (dashed blue line) are shown. Surface-measured RGM concentrations peak during the minima in atmospheric (local and along the transport path) humidity.
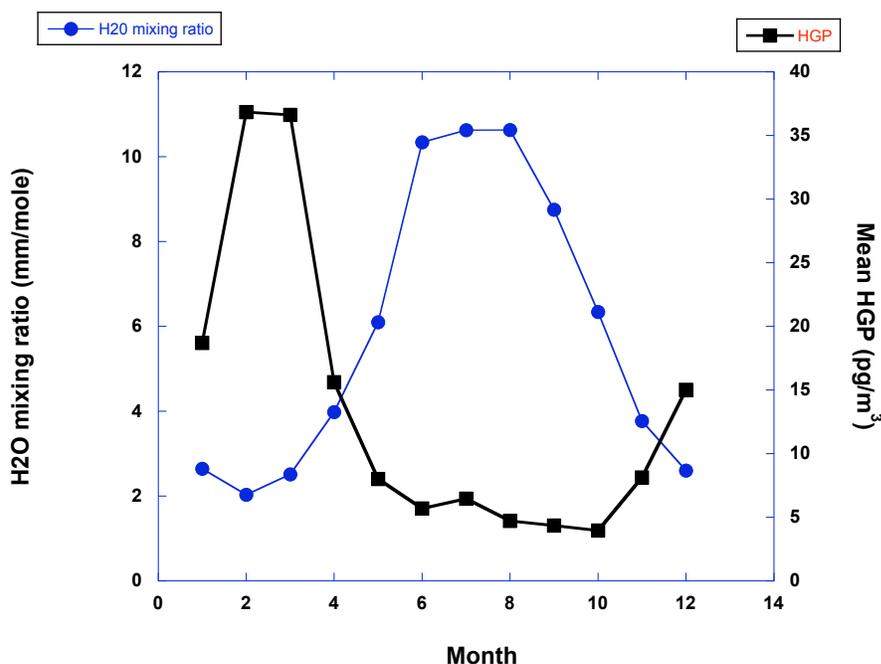
Figure 9. Mean monthly HGP concentrations and the atmospheric water-vapor mixing ratio. HGP concentrations peaked at the minima of atmospheric water vapor. This could indicate that cloud droplets scavenged fewer particles during times of low atmospheric moisture content. Alternatively (see text) this pattern could represent a coincidence between favored trajectories for HGP during winter when the water-vapor mixing ratio is low (in part because of more frequent incursions of polar air with low mixing ratios). In other words, the source regions for low H_2O mixing-ratio air and HGP may be similar. Local combustion sources may also contribute to increased HGP during winter.

RGM and HGP concentrations exhibited two distinct temporal patterns that we interpret as driven by either 1) atmospheric mixing processes in conjunction with the balance between deposition and formation reactions and 2) regional transport episodes (Figure 10). On June 22nd and 23rd 2005, the strong diurnal cycles with concentrations returning to near zero at night suggest that dry-deposition processes outpace replenishment via production reactions or mixing of upper-level air during conditions of low atmospheric mixing at night. During the day, mixing (and/or production processes) outpace the deposition rate and allow surface air concentrations to increase. Ozone and PM levels are moderate on these two days and O_3 follows the same pattern as RGM for the same reasons.

The record from June 24th through June 26th, 2005 illustrates a typical regional transport episode with O_3, and RGM rising together and PM increases lagging slightly (Figure 10). The transport-event signature is the maintenance of moderate to high concentrations overnight. The daytime peaking during a transport event likely indicates additional production during those hours due to photochemistry or the mixing down to the surface of higher concentrations being transported

at higher levels in the atmosphere. These two patterns are repeated again and again throughout the observation record.
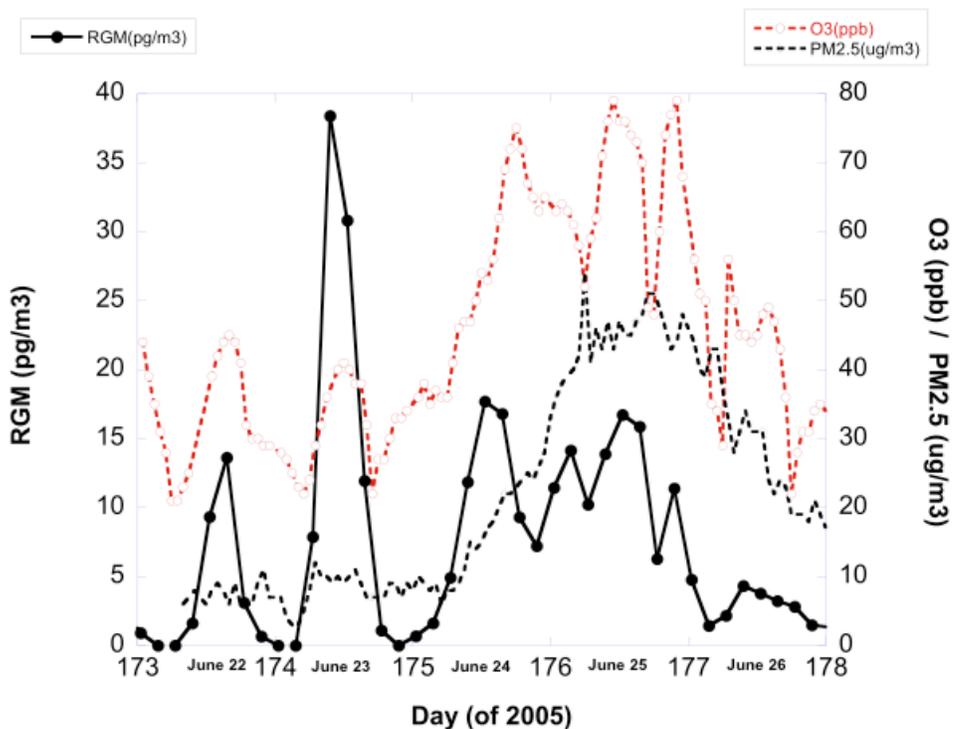

Figure 10. Examples of the two primary temporal patterns of RGM and HGP (RGM only shown here). June 22nd and 23rd illustrate the "mixing/production" pattern, while June 24th through 26th illustrate the patterns associated with regional transport events. Ozone (measured at Underhill) and PM$_{2.5}$ concentrations (measured at Burlington, VT) courtesy of VTANR-APCD.
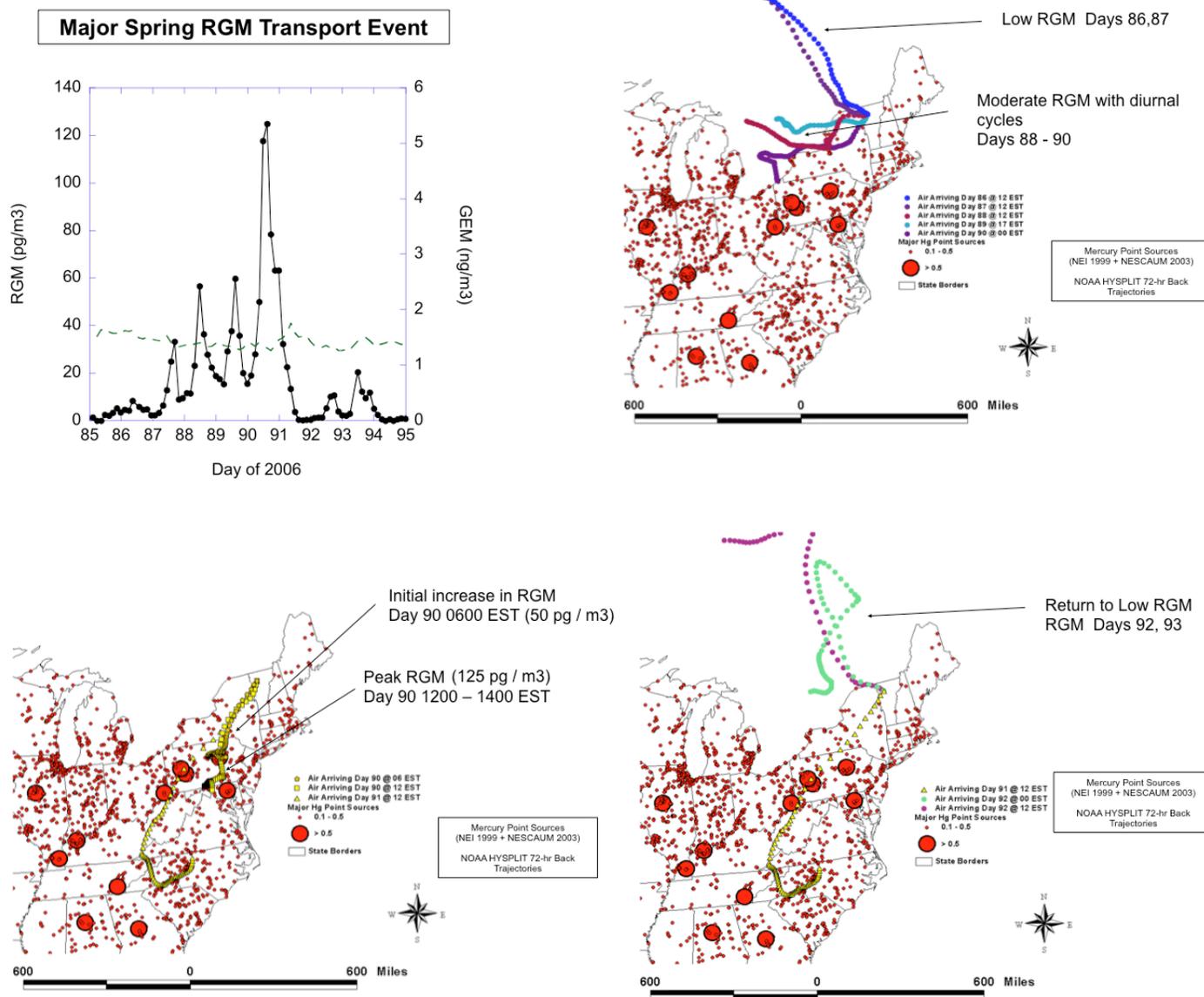
Figure 11. Example of a major RGM transport event in the spring of 2006. The trajectory symbols represent the hourly positions of air in transit to Underhill over the 72-hour preceeding collection of a specific air sample. The time course of RGM concentrations at Underhill is shown in the top left panel. Emissions data courtesy of Mark Cohen (NOAA).

Our confidence in the identification of regional transport events contributing mercury from distant sources to Northern New England is strengthened by detailed air-mass back-trajectory studies of individual events. For example, we present the trajectory analysis of a major RGM transport event that occurred in the spring of 2006 (Figure 11). Prior to the event (days 85-87) low RGM values were observed and air-mass back-trajectories calculated with the NOAA HYSPLIT model indicate air arriving at Underhill had traversed Quebec. On days 88-90, air began arriving from southern Ontario and western New York. RGM levels increased, exhibited strong diurnal cycles, and concentrations failed to return to zero during the night. Days 90 and 91 saw some of the highest RGM levels observed at Underhill up to 125 pg/m^3 (occurring overnight, rather than during

mid-day). Air arriving at Underhill during these samples had recently traversed the RGM emissions-rich region of PA and NJ (Figure 11). Moreover, the trajectory analysis showed that the arriving air mass dwelled for a considerable length of time over specific known major RGM sources, and then began a fairly rapid movement to the receptor. This analysis strongly suggests that several major stationary RGM emission sources (primarily EGUs) in Pennsylvania are responsible for episodically high RGM concentrations and deposition in Northern New England. As discussed elsewhere in this report, these high concentration episodes are responsible for the majority of annual dry deposition. On days 92 and 93, after the passage of a front, air arriving at the receptor was again coming from Quebec and exhibited much lower RGM concentrations with nocturnal values falling to zero (Figure 11).

The relatively long (26-months) and continuous record of high-temporal resolution (every 3-hours) measurements permits unique analysis opportunities for understanding the atmospheric chemistry and regional transport of mercury. These analyses are discussed in detail in the following section.

Identification of potential sources of atmospheric mercury measured at Underhill, VT using Continuous Potential Source Contribution Analysis (CPSCA)

Potential source area identification using single pollutant data is generally conducted using potential source contribution function analysis (PSCF, e.g. Lai et al. 2007). PSCF was developed in the context of moderate-time integration sampling (e.g. 24-hr accumulated samples) where there may be multiple back trajectories contributing to one sample as meteorological conditions change over a 24-hour period. Often this type of sample is collected infrequently (e.g. IMPROVE every 6th-day 24-hr integrated sample). PCSF analysis quantifies the potential for a source region to contribute to the sample by determining the number of instances that a back-trajectory associated with pollutant concentrations above a criterion value measured at a receptor crosses the source region. The number of trajectory intersections are normalized to create a probability (0 to 1) of the source region contributing to a pollutant concentration measurement above the criterion value at the receptor. Depending on the number of pollutant samples available, length of back-trajectories used, and grid size for the potential source fields, a relatively small number of sample-trajectory pairs contribute to the assessment of the potential contribution of each source-field grid cell. A limitation of conventional PSCF analysis is the selection of the concentration criterion that can be arbitrary. Information from trajectories associated with concentrations less than the criterion value is lost.

We adapted earlier methods of source identification for this study (the "upwind average" Poirot and Wishinski 1985 and the "Kenski" method Kenski 2004) and refer to this method as continuous potential source contribution analysis (CPSCA). CPSCA takes advantage of the very large number of samples produced by semi-continuous high-time resolution analyzers (5-minute to hourly or 2-hour samples) for pollutants such as continuous fine particle, ozone, SO_2, NO_X, and mercury analyzers. In addition to the increased number of samples provided by semi-continuous analyzers, each sample can be directly associated with a specific air-mass back trajectory as such back-trajectories rarely differ significantly over the course of such short sample durations. CPSCA makes use of data from trajectories associated with all samples at all times and all observed concentrations, so no information is lost.

Air-mass back-trajectories of 72-hours duration are calculated with hourly endpoints reported using the NOAA HYSPLIT model (Draxler and Rolph 2003) with vertical mixing and the EDAS 40-km meteorological data. With a large number of samples collected continuously representing several years, trajectory endpoints are well distributed spatially and temporally. Thus most locations on the potential source field grid have been sampled multiple times in multiple seasons (sometimes hundreds or thousands of times) by back-trajectories associated with different samples.

Observed local and extracted EDAS meteorological data, along with the observed pollutant concentrations, are associated with each trajectory endpoint arising from a specific sample. The trajectory endpoint-associated data are summarized by source-field grid cell. The choice of grid-cell size influences both the spatial resolution of potential sources and the number trajectory endpoints representing each grid cell. For this analysis data were aggregated by 1-degree latitude and longitude. Data aggregation by grid cell included the mean and maximum of all receptor concentrations associated with trajectories passing through that grid cell. Additional statistics (e.g median, quantiles, even measures of variation) may be used. Gridded data are interpolated to a potential surface using the 6 nearest-neighbor cells with linear distance weighting.

When plotted, the aggregated data display a map of receptor conditions associated with air mass passage over the potential source domain. This type of map immediately conveys the average or maximum concentration (or any other appropriate statistic describing the pollutant or meteorological conditions) at the receptor potentially contributed by sources from a given location. The local and EDAS-extracted meteorological data may be used to inform, stratify, or constrain the analysis based on known or suspected influences of meteorology on pollutant concentrations during transport (e.g. washout due to rain, gas-particle partitioning based on humidity, oxidation/reduction based on sunlight, upper-air entrainment, etc.). For example, for a rapidly dry-depositing species such as RGM or HNO_3, where the dry-deposition velocity is strongly dependent on wetness, data from periods with a wet surface may be excluded.

Contoured pollutant emissions values are overlaid on the unconstrained or constrained receptor concentration source-field maps to explore the correspondence between potential source fields for a given receptor concentration and emissions location and magnitude. With appropriate gridding of emissions data and CPSC data, spatial correlations of emissions with receptor conditions can be calculated with image processing tools for specific regions of the domain or along specific transects through the grid.

Summary of CPSCA Method Steps

1. 72-h air-mass back-trajectories with hourly end-points are calculated for every sample (2 hours sample duration or less) representing the mid point in time of each sample. Trajectories are calculated using the NOAA HYSPLIT model with vertical mixing and the EDAS 40-km meteorological data.

2. Trajectory statistics (total rain, solar flux and average T, Theta, height, mixing height, pressure level, etc.) are extracted from each trajectory.

3. EDAS meteorological information such as mixing depth is extracted at the receptor location for every sample.

4. Local surface average meteorological measurements for every sample at the receptor are compiled.

5. Receptor pollutant concentrations and the EDAS and local observed meteorology are assigned to each hourly trajectory endpoint associated with each sample.

6. The trajectory endpoint-associated data are summarized by source-field grid cell. The choice of grid-cell size influences both the spatial resolution of potential sources and the number trajectory endpoints representing each grid cells. Data aggregation by grid cell includes the mean and maximum of all receptor concentrations (or met parameter) associated with trajectories passing through that grid cell. The median or specific quantiles could also be used. Gridded data are interpolated to a potential surface using the 6 nearest-neighbor cells with linear distance weighting.

7. The aggregated data are plotted to display a map of receptor conditions associated with air mass passage over the potential source domain. This type of map immediately conveys the average or maximum (or other statistic) concentration (or met parameter) at the receptor potentially influenced by sources from a given location.

8. Specific pollutant emissions data are then overlaid on the CPSC map to assess spatial correspondence and emissions intensity correspondence between potential source locations and conditions (various statistics of the measured pollutant concentrations) at the receptor.

9. With appropriate gridding of emissions data and CPSC data, spatial correlations of emissions with receptor conditions can be calculated with image processing tools for specific regions of the domain or along specific transects through the grid.

Application of CPSCA to Underhill Ambient Mercury Data

This section describes the application of CPSCA to data collected using the Tekran Ambient Air Mercury Speciation System deployed at the Underhill, VT Air Quality Site. In the data set considered here there are 8,296 2-hour samples from a 26-month period. A 72-hour air-mass back-trajectory with hourly end-points reported was calculated using the NOAA HYSPLIT model (Draxler and Rolph 2003) with vertical mixing for the center of each 2-hour sample period. The starting height was set to 200 m above model terrain height (~300 m for model terrain at the receptor, actual receptor elevation = 400 masl, approximate start height 500 masl). The start height of 500-meters was selected based on prior experience with calculations of trajectories for this receptor location in complex terrain. There were 588,285 trajectory end points that could each be associated with a concentration measurement at the receptor (Underhill, VT). Because all samples were used, and because the samples were nearly continuous and evenly spaced in time, multiple trajectories "sampled" or "represented" 2/3 of North America and the eastern Atlantic Ocean (Figure 12).

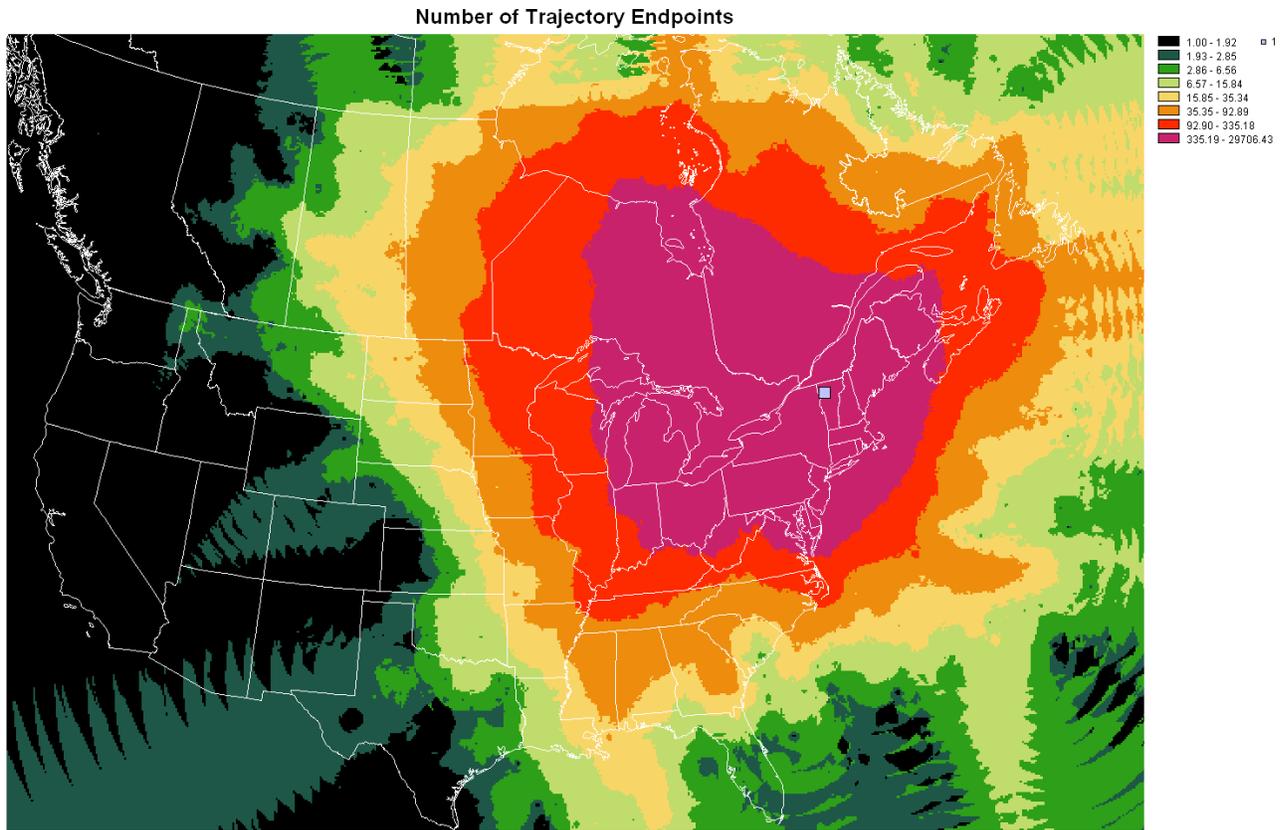**Number of Trajectory Endpoints**

Figure 12. Number of trajectory endpoints at a grid cell location. The blue square represents the receptor location (Underhill, VT). Since trajectories were calculated every 3 hours for a 26-month period, this map shows the frequency (number of endpoints) with which air arriving at the receptor traversed a given location up to 72 hours before arrival.

The CPSC map for the average RGM at Underhill indicates potential major sources in a corridor from Tennessee through West Virginia and Pennsylvania (Figure 13). Important sources are also indicated in New Jersey and Southern New York. A potential significant source is indicated as far away as northeast Texas. While significant emissions sources exist in northeast Texas (discussed below), we remain cautious about assigning importance to potential source contributions indicated in areas sampled by only a small number of trajectories (see Figure 12). A possible major source is indicated in Newfoundland Canada. A major potential marine source region is indicated in the western Atlantic Ocean east of Cape Cod. A less significant marine source is indicated from the region of Hudson Bay. The CPSCA indication of important marine RGM sources is consistent with identification of important marine RGM sources in recent model simulations by Sillman et al. (http://www.htap.org/meetings/2007/2007_01/presentations/ Thursday%20afternoon/Sillman_IHTP_Geneva2007.pdf). However, the location of the marine sources identified by this study differs from the locations identified by Sillman. This may be a result of the specific modeling time periods considered.

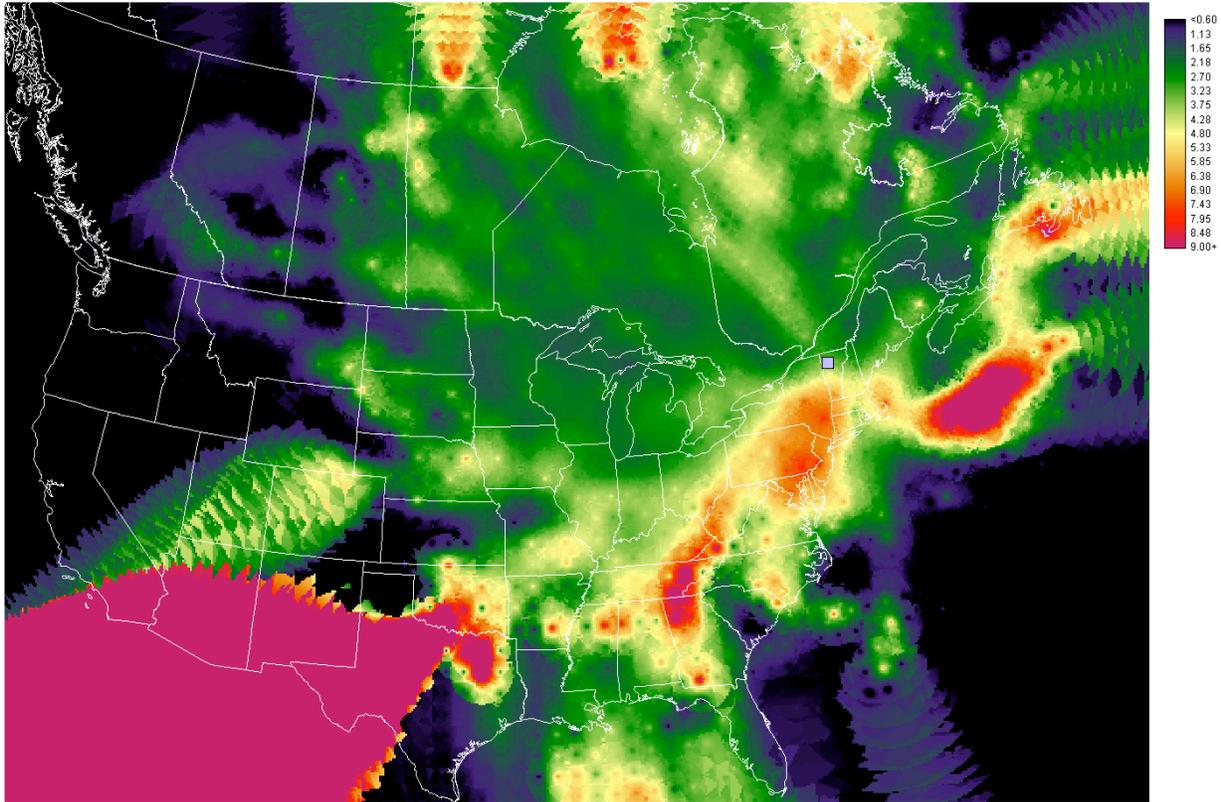72-h Trajectory Mean RGM (pg/m3) at Receptor (VT99)

Figure 13. CPSC map for RGM sources depicting the potential contribution of a given location to average concentrations of the indicated value at the receptor (Underhill, VT – indicated by the blue square. Green indicates source areas contributing air arriving with an average concentration of 2-3 pg/m^3, while red areas indicate source areas contributing air arriving with an average concentration of 7 pg/m^3 or greater. *SPECIAL NOTE: this report reflects work in progress. As this material is revised for publication figures will be improved. We plan to mask these figures at a specific value of number of trajectory endpoints per grid cell. This will eliminate the visual artifacts such as the large red area extending from western Texas where only a few trajectories endpoints were located (see Figure12). The analysis discussed in this report ignores or discounts these artifacts. Please try to not be distracted by them. We did not have time to remake all the figures by the report submission deadline.*

Speciated mercury emissions estimates (Cohen et al. 2004) representing 1999 emissions inventories for the US and Canada were used to determine the spatial and emissions magnitude correspondence with receptor concentrations associated with a given potential source location. Incinerator (municipal waste and medical) emissions, which are known to have been reduced dramatically since 1999, were excluded to avoid confounding the analysis. Emissions (point and area sources) were gridded at 0.1-degree latitude and longitude resolution. Contours of emissions values were generated from the grid and were overlaid on the receptor concentration source-field maps to explore the correspondence between potential source fields for a given receptor concentration and emissions location and magnitude (Figure 14).
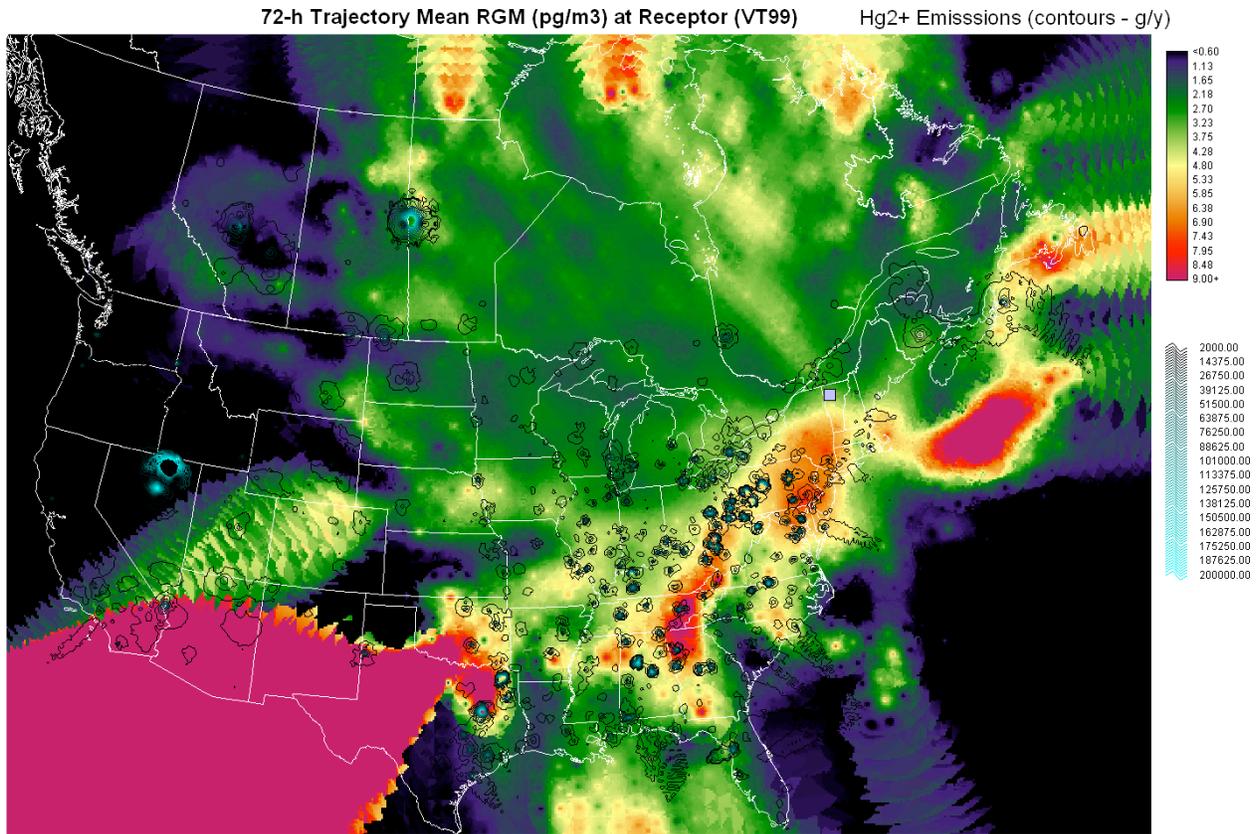
Figure 14. Overlay of 1999 US and Canada Hg^{2+} (RGM) emissions (courtesy of Mark Cohen, NOAA-ARL) on the CPSC map for mean RGM at Underhill, VT. Emissions (g/y) are contoured with light blue indicating the highest emission rates. *SPECIAL NOTE: this report reflects work in progress. As this material is revised for publication figures will be improved. We plan to mask these figures at a specific value of number of trajectory endpoints per grid cell. This will eliminate the visual artifacts such as the large red area extending from western Texas where only a few trajectories endpoints were located (see Figure 12). The analysis discussed in this report ignores or discounts these artifacts. Please try to not be distracted by them. We did not have time to remake all the figures by the report submission deadline.*

There was an excellent spatial correspondence between emissions source locations and intensity and the potential source areas for a given average RGM concentration at the receptor (Figure 14). The different densities and intensities of sources appear clearly related to the average RGM concentration arriving at the receptor attributable to a given source field. It is noteworthy that very large and very distant sources (northeast Texas and the Flin-Flon base-metal smelter in Manitoba are indicated as potential sources by the CPSC map for mean RGM concentration. The potential contributions from these distant sources is more clearly identified by the CPSC map for the maximum RGM concentrations from a given source-field location (Figure 15). The maximum RGM concentration CPSC map depicts major plume "hits" at Underhill associated with a source field location. It should be noted that because air arriving from any moderate-range or long-range source must traverse the relatively source-free area within a few hundred km of the receptor, this near-receptor area is indicated as potentially "contributing" high concentrations of RGM – especially on the maximum concentration maps. The interpretation of the maximum concentration map display close to the receptor (when there are no known or suspected sources) should be that of a transport route.
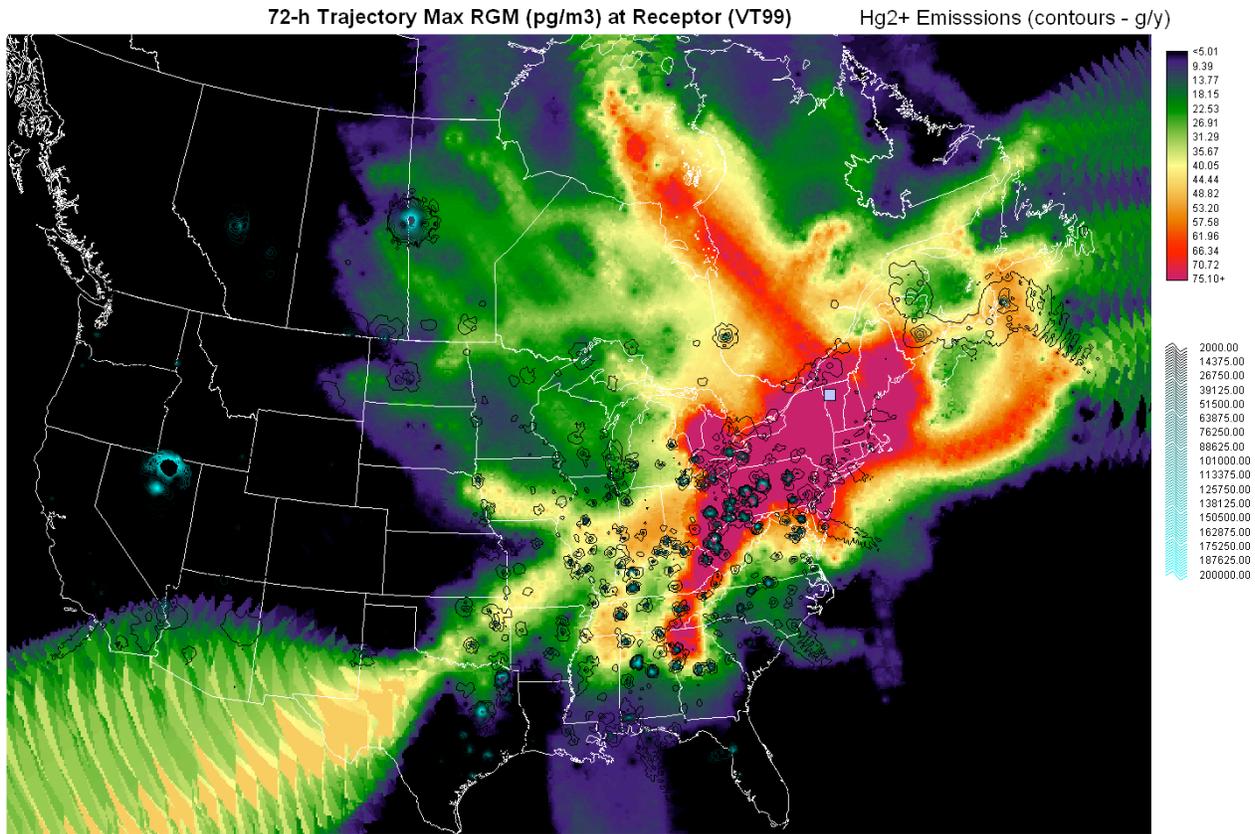
Figure 15. CPSC map of maximum RGM concentration observed at Underhill for air traversing a given location. 1999 US and Canada Hg^{2+} (RGM) emissions (courtesy of Mark Cohen, NOAA-ARL) are overlaid for reference. Using the maximum RGM value highlights specific trajectories associated with major transport events more than the average RGM CPSC map. *SPECIAL NOTE: this report reflects work in progress. As this material is revised for publication figures will be improved. We plan to mask these figures at a specific value of number of trajectory endpoints per grid cell. This will eliminate the visual artifacts such as the large highlighted area extending from western Texas where only a few trajectories endpoints were located (see Figure 12). The analysis discussed in this report ignores or discounts these artifacts. Please try to not be distracted by them. We did not have time to remake all the figures by the report submission deadline.*

The CPSC maps for mean (Figure 16) and maximum (Figure 17) HGP concentrations at Underhill indicate a different set of locations for major particulate mercury source areas consistent with the HGP emissions data. The potential impact of the Flin-Flon base-metal smelter in Manitoba as a source of HGP arriving at Underhill is evident in both maps. HGP sources appear to be mainly to the N and NW of the receptor while RGM sources are predominantly to the S and SW. There are indications of an unknown source along the Mississippi River in eastern Iowa. A possible marine source in the Atlantic is indicated as well for moderate (50-75 pg/m^3) HGP events.

The CPSC map for mean GEM concentrations at Underhill indicates yet a different pattern of contributing source areas (Figure 18). A more diffuse contributing zone from the W through the S is peppered with industrial and power-generation GEM sources. A potential marine source is indicated along the coast from Florida through the Carolinas. The CPSC map for maximum concentrations (big "hits") indicates major sources in the emission-rich Ohio-River corridor on through to major sources in eastern Texas are responsible for the highest GEM concentrations observed at Underhill (Figure 19).
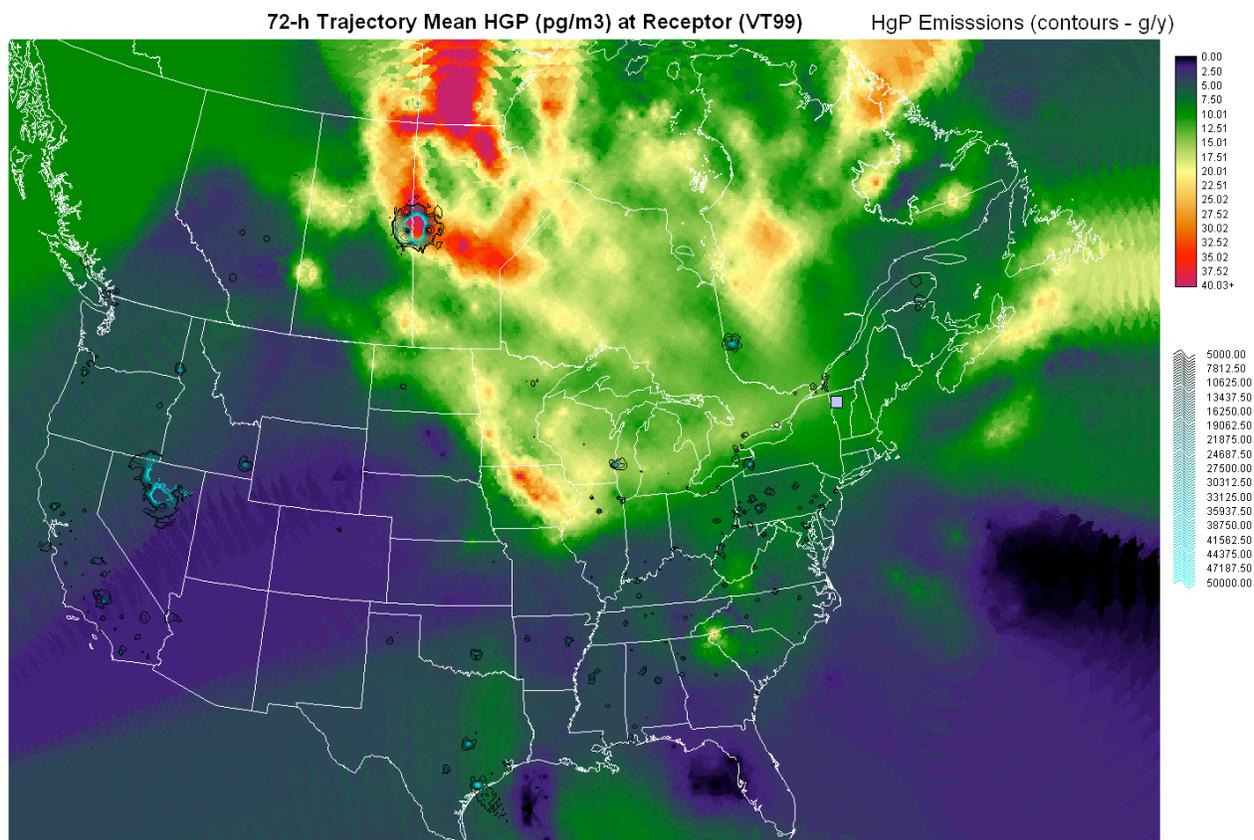
Figure 16. CPSC map for HGP sources depicting the potential contribution of a given location to average concentrations of the indicated value at the receptor (Underhill, VT – indicated by the blue square. Green indicates source areas contributing air arriving with an average concentration of 7-15 pg/m^3, and red areas indicate source areas contributing air arriving with an average concentration of 30 pg/m^3 or greater. 1999 US and Canada HgP emissions (courtesy of Mark Cohen, NOAA-ARL) are overlaid for reference. *SPECIAL NOTE: this report reflects work in progress. As this material is revised for publication figures will be improved. We plan to mask these figures at a specific value of number of trajectory endpoints per grid cell. This will eliminate the visual artifacts such as the large highlighted area northwest of Hudson Bay where only a few trajectories endpoints were located (see Figure 12). The analysis discussed in this report ignores or discounts these artifacts. Please try to not be distracted by them. We did not have time to remake all the figures by the report submission deadline.*
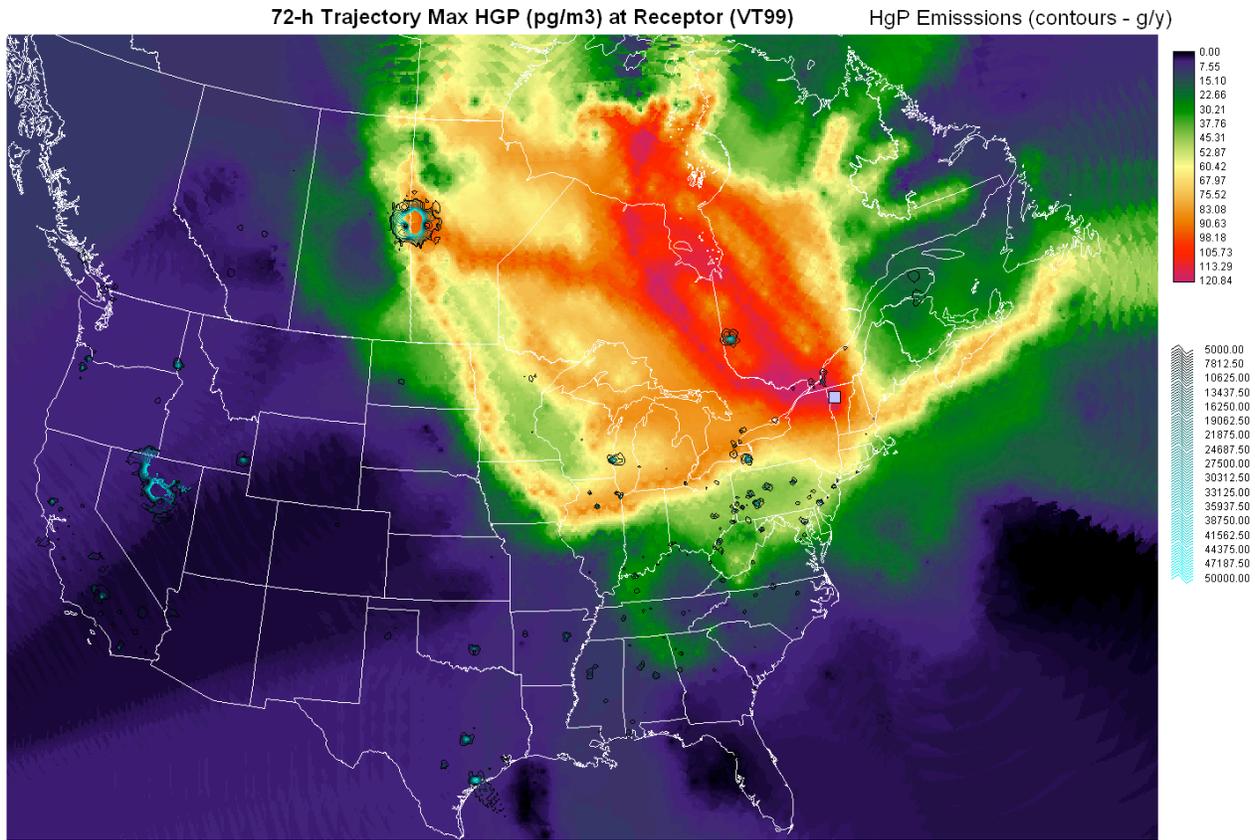
Figure 17. CPSC map of maximum HGP concentration observed at Underhill for air traversing a given location. 1999 US and Canada HGP emissions (courtesy of Mark Cohen, NOAA-ARL) are overlaid for reference. Using the maximum HGP value highlights specific trajectories associated with major transport events more than the average HGP CPSC map. The large Manitoba base-metal smelter is indicated as a major HGP source via multiple transport paths. A possible marine source in the Atlantic is indicated as well for moderate (50-75 pg/m^3) HGP events. *SPECIAL NOTE: this report reflects work in progress. As this material is revised for publication figures will be improved. We plan to mask these figures at a specific value of number of trajectory endpoints per grid cell. This will eliminate the visual artifacts such as the large highlighted area northwest of Hudson Bay where only a few trajectories endpoints were located (see Figure 12). The analysis discussed in this report ignores or discounts these artifacts. Please try to not be distracted by them. We did not have time to remake all the figures by the report submission deadline.*
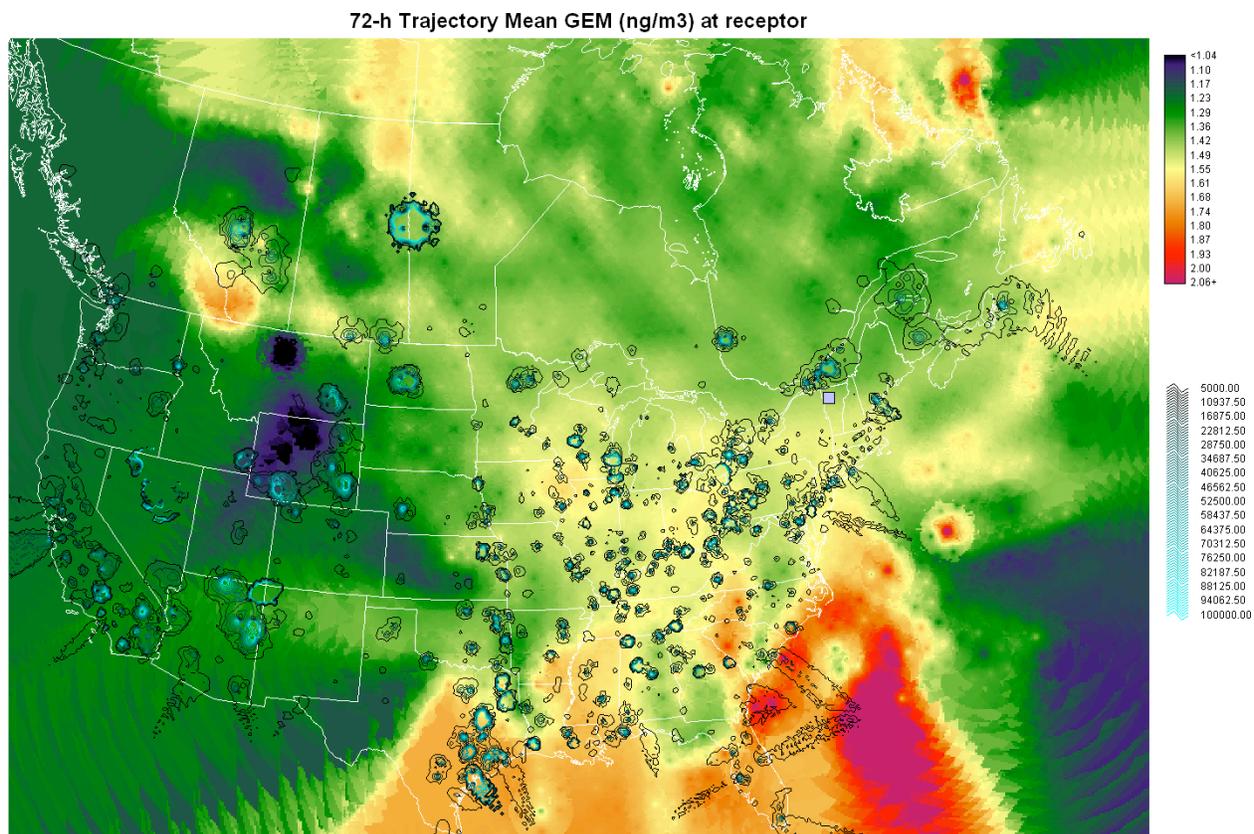
Figure 18. CPSC map for GEM sources depicting the potential contribution of a given location to average concentrations of the indicated value at the receptor (Underhill, VT – indicated by the blue square. Green indicates source areas contributing air arriving with an average concentration of 1.2-1.4 ng/m³(gobal background), and red areas indicate source areas contributing air arriving with an average concentration of 1.8 ng/m³ or greater. 1999 US and Canada GEM emissions (courtesy of Mark Cohen, NOAA-ARL) are overlaid for reference. *SPECIAL NOTE: this report reflects work in progress. As this material is revised for publication figures will be improved. We plan to mask these figures at a specific value of number of trajectory endpoints per grid cell. This will eliminate the visual artifacts such as the large highlighted area in the western US where only a few trajectories endpoints were located (see Figure 12). The analysis discussed in this report ignores or discounts these artifacts. Please try to not be distracted by them. We did not have time to remake all the figures by the report submission deadline.*
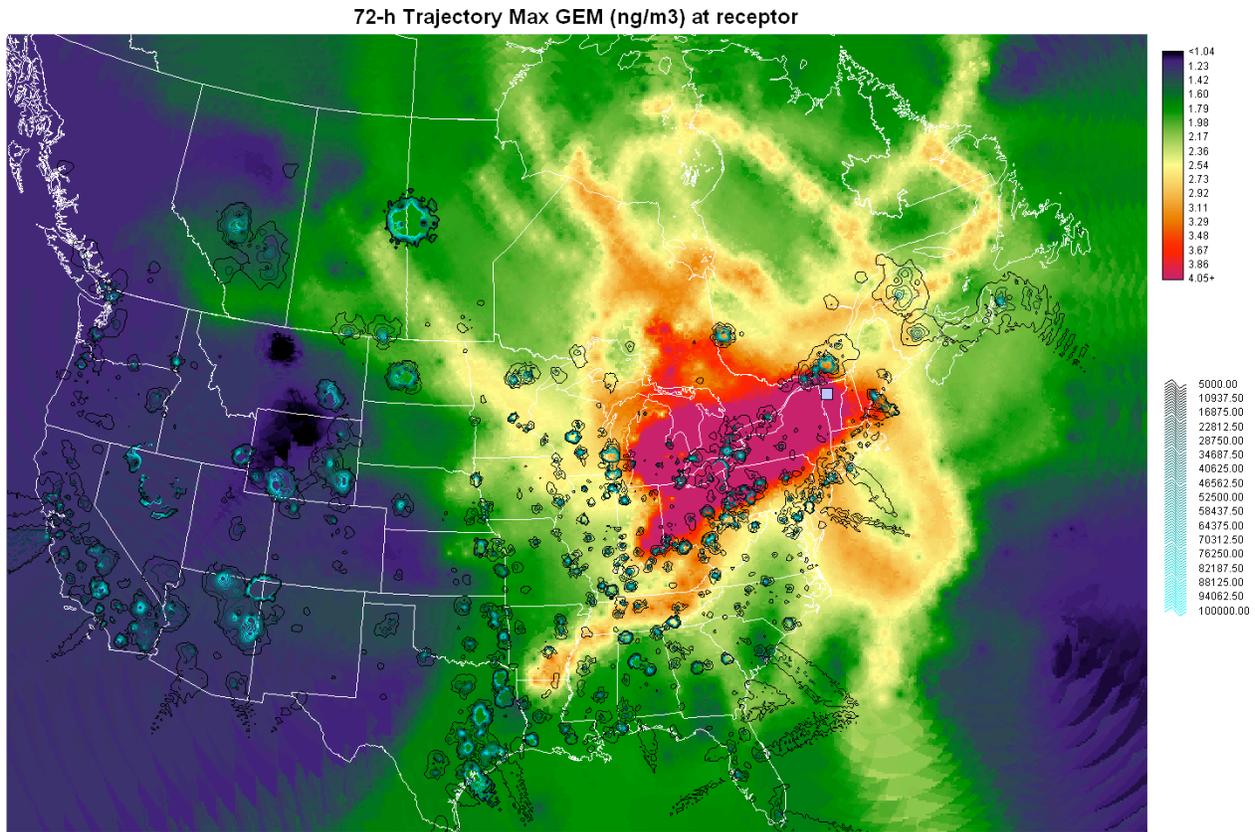
Figure 19. CPSC map of maximum GEM concentration observed at Underhill for air traversing a given location. 1999 US and Canada GEM emissions (courtesy of Mark Cohen, NOAA-ARL) are overlaid for reference. Using the maximum GEM value highlights specific trajectories associated with major transport events more than the average GEM CPSC map. *SPECIAL NOTE: this report reflects work in progress. As this material is revised for publication figures will be improved. We plan to mask these figures at a specific value of number of trajectory endpoints per grid cell. This will eliminate the visual artifacts such as the highlighted areas in the western US where only a few trajectories endpoints were located (see Figure 12). The analysis discussed in this report ignores or discounts these artifacts. Please try to not be distracted by them. We did not have time to remake all the figures by the report submission deadline.*

The analysis described above demonstrates the capability and sensitivity of CPSCA for source identification and attribution of atmospheric mercury. To illustrate the generality of the method, CPSCA was conducted for the ambient water vapor mixing ratio as measured at Underhill for the same set of trajectories as the mercury observations. The CPSC map of potential water vapor sources is intuitively reasonable with major source regions identified off the eastern Atlantic coast and in the Gulf of Mexico (Figure 20). A more modest potential source of water vapor is indicated in the region of the Great Lakes and another moderate source from Hudson Bay. It seems likely this method can be fruitfully applied to other continuous pollutant data (SO_2, O_3, $PM_{2.5}$ by TEOM) from Underhill and other locations.

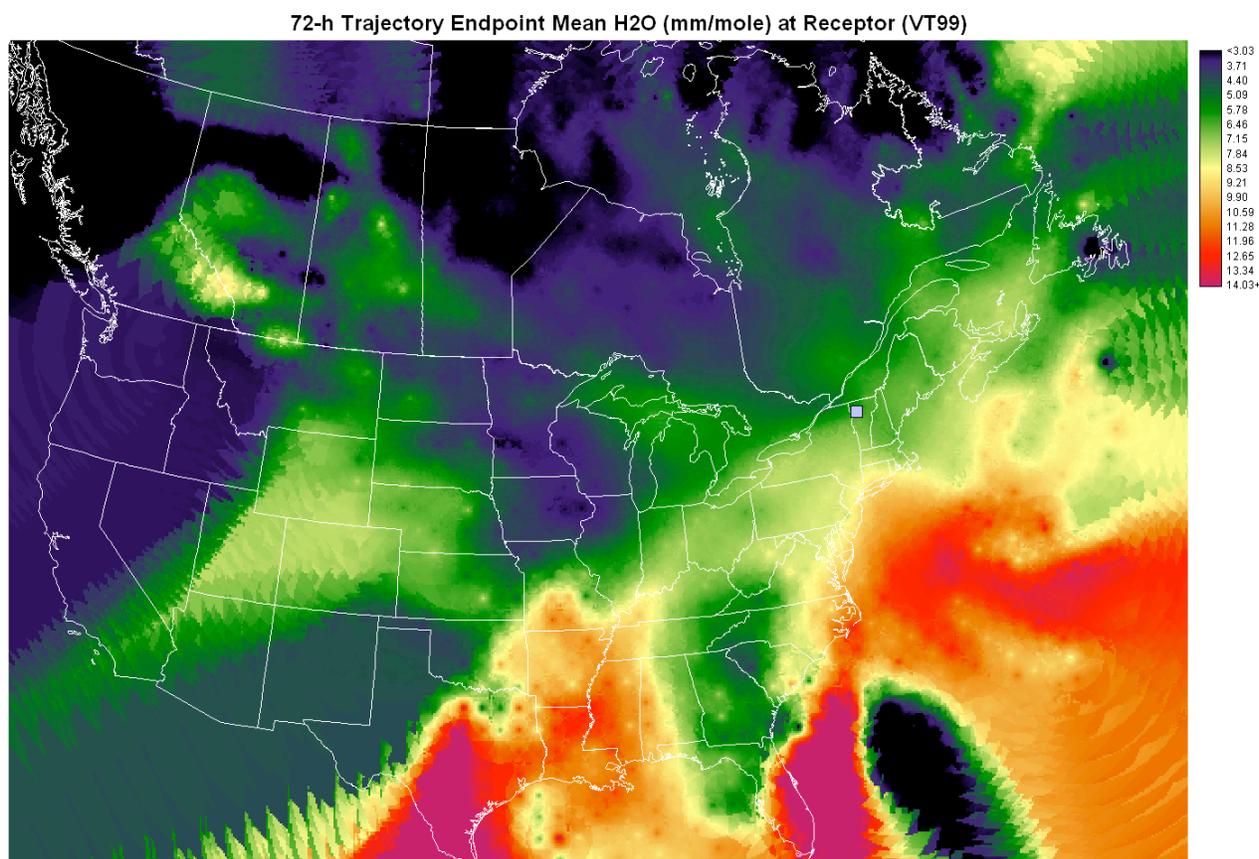72-h Trajectory Endpoint Mean H2O (mm/mole) at Receptor (VT99)

Figure 20. CPSC map for mean water-vapor mixing ratio. The anticipated source regions of the Atlantic Ocean and Gulf of Mexico are clearly indicated. The Great Lakes Region is indicated as a moderate source. *SPECIAL NOTE: this report reflects work in progress. As this material is revised for publication figures will be improved. We plan to mask these figures at a specific value of number of trajectory endpoints per grid cell. This will eliminate the visual artifacts such as the highlighted areas in the western US where only a few trajectories endpoints were located (see Figure 12). The analysis discussed in this report ignores or discounts these artifacts. Please try to not be distracted by them. We did not have time to remake all the figures by the report submission deadline.*

Ambient Atmospheric Mercury Speciation Summary

The ambient concentrations of the 3 major forms of atmospheric mercury GEM, HGP, and RGM were successfully characterized. This information allows improved dry-deposition modeling and dry-deposition estimates for the Lake Champlain Basin. We were able to interpret seasonal and diurnal variations of GEM, RGM and HGP concentrations in terms of observed meteorological influences and regional transport from anthropogenic and natural sources. Both individual transport-event analyses and the CPSC analysis of the full 26-month suggest that out-of-region sources are dominantly responsible for the moderate and highest concentrations of RGM, HGP, and GEM observed at Underhill, Vermont. Thus, reductions of mercury dry deposition will depend on successful reductions of out-of-state and out-of-region sources. The information generated through this project will be of great value to atmospheric modelers attempting to predict changes in mercury deposition from changes in emissions.

References

Cohen, M., R. Artz, R. Draxler, P. Miller, D. Niemi, D., D. Ratte, M. Deslauriers, R. Duvar, R., Laurin, J. Slotnick, T. Nettesheim, and J. McDonald. (2004) Modeling the atmospheric transport and deposition of mercury to the Great Lakes. Environmental Research 95:, 247-265.

Draxler, R.R. and Rolph, G.D., 2003. HYSPLIT (HYbrid Single-Particle Lagrangian Integrated Trajectory) Model access via NOAA ARL READY Website (http://gus.arlhq.noaa.gov/ready/open/hysplit4.html). NOAA Air Resources Laboratory, Silver Spring, MD.

Kenski, D.M. (2004). Quantifying Transboundary Transport of PM2.5: A GIS Analysis. *Proc. AWMA 97th Annual Conf.*, Indianapolis (June 2004).

Lai, S.-o , T. M. Holsen, P. K. Hopke, and P. Liu. (2007) Wet deposition of mercury at a New York state rural site: Concentrations, fluxes, and source areas. *Atmos. Environ.* 41:4337-4348.

Lindberg, S. E., and W.J. Stratton. 1998. Atmospheric mercury speciation: Concentrations and behavior of reactive gaseous mercury in ambient air. *Envir. Sci. & Technol.* 32:49-57.

Miller, E.K., VanArsdale, A., Keeler, G.J., Chalmers, A., Poissant, L., Kamman, N., and Brulotte, R. (2005) Estimation and Mapping of Wet and Dry Mercury Deposition across Northeastern North America. *Ecotoxicology* 14, 53-70.

Poirot, R.L. and P.R. Wishinski (1985). Regional apportionment of ambient sulfate contributions to a remote site in northern VT. *Transactions APCA Int. Spec. Conf. on Receptor Modeling: Real World Issues and Applications*, T.G. Pace, Ed., pp. 239-250, Williamsburg, VA.